Phys. Status Solidi B **246**, No. 11–12, 2740–2743 (2009) / **DOI** 10.1002/pssb.200982352

physica status solidi b
www.pss-b.com
basic solid state physics

Quantitative composition of a single-walled carbon nanotube sample: Raman scattering versus photoluminescence

Sebastian Heeg[*,1], **Ermin Malić**[2], **Cinzia Casiraghi**[1], **and Stephanie Reich**[1]

[1] Freie Universität Berlin, Arnimallee 14, 14195 Berlin, Germany
[2] Technische Universität Berlin, Hardenbergstrasse 36, 10623 Berlin, Germany

Received 3 June 2009, revised 17 August 2009, accepted 21 August 2009
Published online 13 November 2009

PACS 63.22.Gh, 73.63.Fg, 78.30.Na, 78.67.Ch

[*] Corresponding author: e-mail sebastian.heeg@physik.fu-berlin.de, Phone: +49 30 83856157, Fax: +49 30 83856081

We investigated the spectral data of three carbon nanotube (CNT) species obtained by Raman spectroscopy and photoluminescence (PL) measurements. The corresponding relative signal intensities without further corrections yielded significantly different relative distributions of the CNT species. Theoretical calculations of optical transition probabilities and electron–phonon coupling were included, providing simple models in order to estimate the relative distribution of the three species within the sample. We proposed the product of PL and PL excitation intensities to be a candidate for quantitative analysis of CNT species. Applying the models, we confirmed that both spectroscopic methods agree on one nanotube species dominating the distribution.

1 Introduction Carbon nanotubes (CNTs) are hollow cylinders made of carbon which were first reported in 1991 [1]. Depending on their microscopical structure, described by the chiral index (n_1, n_2), they are either metallic or semiconducting [2]. Being regarded as one-dimensional physical systems, they show strongly structured optical spectra. Hence, optical spectroscopy like Raman scattering and photoluminescence (PL), which make use of properties specific to each chiral index such as electronic and phonon energies, are prime tools in CNT characterization. The growth processes of CNTs yield samples containing tubes with a variety of different chiralities. The qualitative composition of a CNT sample has been revealed by Raman scattering and PL spectroscopy [3]. The quantitative composition, however, remains an open question. We address this question by comparing the relative signal intensities of three semiconducting CNT species, obtained by the two spectroscopic methods. Including calculations of optical transition probabilities and electron–phonon coupling, we estimate the relative abundance of the species. We concentrate on three semiconducting species with similar optical transition energies E_{22}.

2 Photoluminescence measurements Single-walled nanotubes were HiPCO grown. In order to solubilize the nanotubes in aqueous solution sodium dodecylbenzene sulphonate (SDBS) was added as a surfactant. The measurements were performed using a Fluorolog-3 Spectrofluorometer. A HgXe lamp served as source of light. The PL signals were recorded with an InGaAs detector. The measurements were normalized with respect to the light source intensity using a Si diode. The spectrometer response was normalized using a halogen lamp. The energies E_{22} and E_{11}, referring to excitation and emission, respectively, were assigned to specific chiralities corresponding to the empirical relations by Bachilo et al. [3]. In Fig. 1, we depict the PL excitation (PLE) map of the (7,5), (7,6) and (10,3) nanotubes. The observed signal intensities represent the abundance of the according nanotube species as well as their intrinsic PL intensities.

Usually, either the peak height or the integrated intensity of the signal is interpreted as the PL intensity in the nanotubes literature [4]. For the (7,6) nanotube the latter is indicated by the horizontal line in Fig. 1. The corresponding PL spectrum at a fixed excitation wavelength is shown in Fig. 2. Table 1

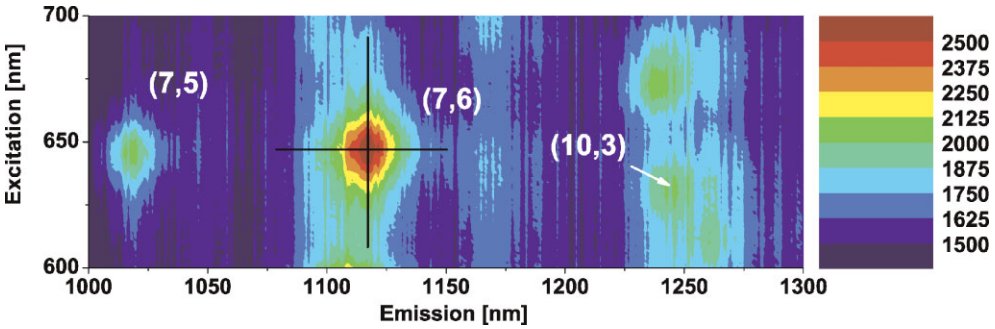

Figure 1 (online colour at: www.pss-b.com) PLE map of the (7,5), (7,6) and (10,3) nanotube. The intensity is decoded by colours. For the (7,6) tube, the spectra for PL (horizontal line) and PLE (vertical line) are indicated.

summarizes the relative integrated PL intensities for the (7,5), (7,6) and (10,3) tubes with respect to their summed intensities. The corresponding analysis for the PLE – indicated by the vertical line in Fig. 1 – yields similar relative intensities at first glance and is shown in Fig. 3. The absolute PL and PLE intensities for each chirality, however, yield different PL/PLE ratios. This is partly due to the fact that the peak height of the PL and PLE spectra do not coincide exactly at the intersection point with a maximal deviation of 5%, which is attributed to the different nature of background for PL and PLE. For the (7,5) and (7,6) nanotubes, the PL intensity exceeds the PLE intensity by 10 and 19%, respectively. For the (10,3) this tendency is reversed. Two additional nanotube species, which are not part of the subset investigated, show varying PL/PLE ratios as well. So far, no dependence of the ratio on diameter, chiral angle or nanotube family has been observed.

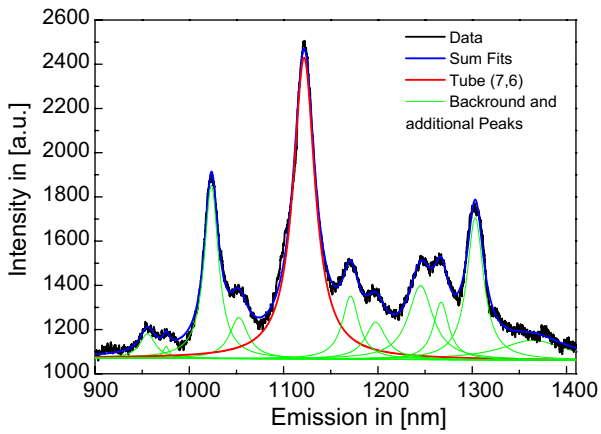

Figure 2 (online colour at: www.pss-b.com) PL spectrum at an excitation wavelength of 648 nm, corresponding to the horizontal line in Fig. 1. The peak that belongs to the (7,6) tube is highlighted in red.

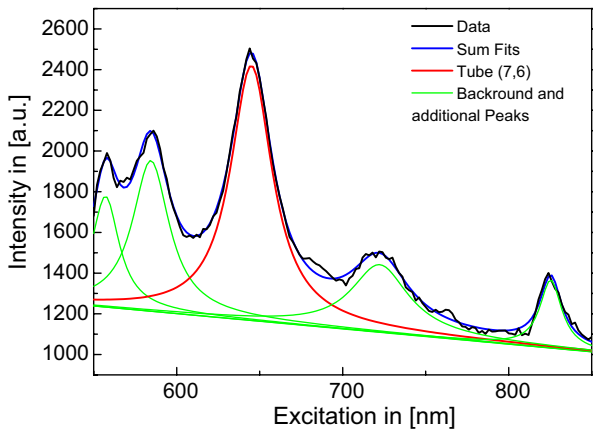

Figure 3 (online colour at: www.pss-b.com) PLE spectrum at an emission wavelength of 1121 nm, corresponding to the vertical line in Fig. 1. The peak that belongs to the (7,6) tube is highlighted in red.

The varying PL/PLE ratio indicates that the PLE intensities are specific to nanotube species and have to be taken into account in order to obtain the abundance of different species from PL experiments. We propose the product of PL and PLE intensities as a candidate, as it incorporates both contributions in equal measure. The relative intensities obtained by the product of PL and PLE are summarized in Table 1.

To estimate the abundance of nanotube species from the product of PL and PLE, we need to model absorption, relaxation and emission cross-sections. The absorption of light, referring to the excitation from the ground state to the bright excitonic state eh_{22}, is determined by the oscillator strength of the excitonic transition $\alpha(E_{22})$, which has been calculated by Malić and Berlin [5]. The relaxation from eh_{22} to the first bright excitonic state eh_{11} is mediated mainly by excitonic resonances [6] and/or electron–phonon coupling [7]. As the relaxations

Table 1 Top: relative intensities obtained by PL, PLE and ratio. Note that the absolute PL intensity exceeds the PLE intensity, leading to a PL/PLE ratio of 1.1 although their relative intensities are the same in case of the (7,5) tube. Bottom: relative intensities of PL × PLE and estimated abundance $\mathcal{A}_{i,j}$.

	(7,5)	(7,6)	(10,3)	(8,3)	(8,7)
intensity PL	26.1%	65.0%	8.9%	–	–
intensity PLE	26.1%	60.2%	13.6%	–	–
ratio PL/PLE	1.10	1.19	0.72	0.81	1.33
PL × PLE	14.5%	83.0%	2.5%	–	–
$\mathcal{A}_{i,j}$ (Eq. 1)	16.3%	81.3%	2.4%	–	–
difference	+1.8%	−1.7%	−0.1%	–	–

occur at a timescale several orders of magnitude faster than the lifetime of the excitonic states [8], they are negligible.[1] The emission intensity depends on the oscillator strength of the excitonic transition $\alpha(E_{11})$, here from the excitonic state eh_{11} to the ground state. The transition probabilities depend strongly on the nanotube family as well as on the chiral angle. The dependence on the latter is less pronounced for $\alpha(E_{11})$ than for $\alpha(E_{22})$.

We estimate the relative abundance $\mathcal{A}_{i,j}$ of each of the nanotubes (i, j) in the subset by correcting the product of the experimentally obtained PL and PLE intensities $I_{i,j}$ (PL) and $I_{i,j}$ (PLE) by the excitonic transition probabilities as

$$\mathcal{A}_{i,j} = \frac{I_{i,j}(\mathrm{PL}) \times I_{i,j}(\mathrm{PLE})}{\alpha_{i,j}(E_{22}) \times \alpha_{i,j}(E_{11})} \sum_{\mathrm{subset}} \frac{\alpha_{i,j}(E_{22}) \times \alpha_{i,j}(E_{11})}{I_{i,j}(\mathrm{PL}) \times I_{i,j}(\mathrm{PLE})}. \quad (1)$$

The estimated abundances are shown in Table 1. The correction by the transition probabilities does not induce significant deviations from the measured relative intensities.

3 Raman measurements The radial breathing mode (RBM) of a single-walled CNT uniquely identifies its chirality. Although some CNTs show very similar RBM frequencies, a correct assignment is ensured by the sharp resonance conditions of the Raman process [9, 10]. For Raman measurements we used a T64000 triple grating Raman spectrometer in combination with an Ar/Kr ion laser. The nanotubes in aqueous solution were dispersed on a Si substrate by spin coating. Figure 4 shows a typical Raman spectrum. The (7,5), (7,6) and (10,3) RBM peaks are highlighted in the figure. We took measurements on different spots on the substrate to verify that the spectra represent the chirality distribution of the nanotubes in solution. The obtained intensities are averaged over all measurements, showing a homogenous distribution of the different chiralities on the substrate.

The Raman resonance profile can be described by [9]

$$I(E_\mathrm{l}) = \left(\frac{c\mathcal{M}}{\hbar\omega_{\mathrm{RBM}}}\right)^2 \left| \frac{1}{E_\mathrm{l} - E_{ii} - i\gamma/2} - \frac{1}{E_l - \hbar\omega_{\mathrm{RBM}} - E_{ii} - \gamma/2} \right|^2, \quad (2)$$

where E_l is the laser energy, E_{ii} the energy of the optical transition and γ the lifetime broadening of the intermediate electronic states. $\mathcal{M}$ contains all matrix elements and c summarizes all remaining factors.

To compare the intensity of the RBM of different CNT species, they have to be compared being excited at the maximum of their resonance curves. We simulate this by scaling the intensity obtained at the given laser energy with respect to maximum intensity. In Fig. 5, the resonance curves of the (7,6) and the (8,3) tubes measured by Maultzsch et al. [9] are shown. The black curve corresponds to the (7,6) tube. At a laser energy of 1.91 eV the Raman intensity of the (7,6) tube is at 89% of its maximum. Hence we multiply the experimentally obtained intensity by

[1] This does not apply for several zig-zag and close to zig-zag tubes due to excitonic quenching [6]. None of them are investigated here.

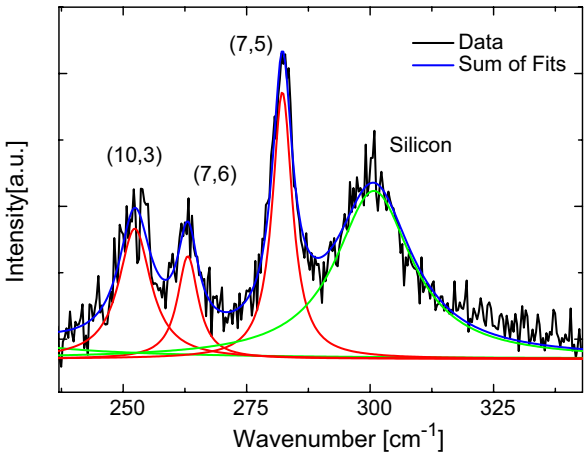

Figure 4 (online colour at: www.pss-b.com) RBM modes of CNTs dispersed on Si at a laser energy of 1.91 eV.

$\mathcal{F}_{(7,6)} = 100\%/89\% = 1.123$, simulating excitation at full resonance. Applying similar scaling factors $\mathcal{F}_{(i,j)}$ to the two other nanotube species yields the relative intensities reported in Table 2.

To estimate the abundance of the different chiralities from the Raman intensity of the RBM, we have to identify the factors which contribute to the chirality specific Raman intensity $I_{R(i,j)}$. The matrix elements summarized in $\mathcal{M}$ of Eq. (2) contain electron–radiation coupling elements for absorption and emission as well as the electron–phonon coupling matrix element M_{22} (the index refers to the CNTs being excited to the second excitonic state). The latter has been calculated amongst others by Jiang et al. [11] for a variety of different nanotube species. M_{22} strongly depends on the chirality. We approximate both terms of the second part of Eq. 2, which corresponds to the Raman resonance conditions, by the excitonic transition probability $\alpha(E_{22})$. All remaining factors such as the electron–photon coupling matrix elements included in $\mathcal{M}$ of Eq. (2), are set constant as

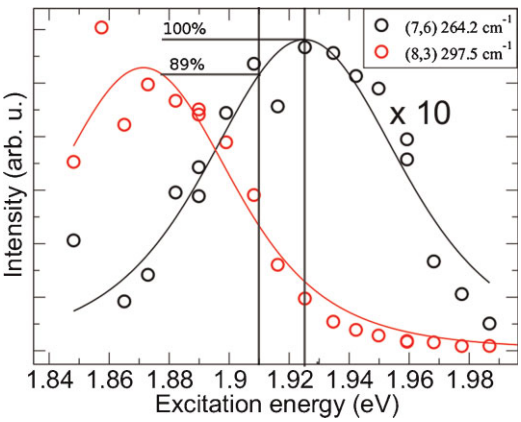

Figure 5 (online colour at: www.pss-b.com) RBM Raman resonance profile of the (7,6) and (8,3) nanotubes measured by Maultzsch et al. [9]. At a laser energy of 1.91 eV, the Raman intensity is at 89% of its maximum.

Table 2 Top: measured relative Raman intensities of the RBMs. Centre: relative intensities after scaling to full resonance with respect to the resonance profile. Bottom: estimated abundance including approximation on chirality specific RBM Raman intensity.

CNT species	(7,5)	(7,6)	(10,3)
experiment	33%	28%	39%
scaled by $\mathcal{F}_{(i,j)}$	46%	20%	34%
$\mathcal{B}_{(i,j)}$ (Eq. (4), corr. by $I_{R(i,j)}$)	12.7%	83.7%	3.6%

they do not depend on the nanotube chirality [2]. Including these correction yields

$$I_{R(i,j)} \propto \left|M_{22(i,j)}\right|^2 \left|\alpha_{(i,j)}(E_{22})\right|^2, \tag{3}$$

for the chirality specific Raman intensity $I_{R(i,j)}$. Dividing the experimentally obtained intensities $I_{(i,j)}$(Exp) by $I_{R(i,j)}$ yields the estimated abundance $\mathcal{B}_{(i,j)}$ for each nanotube species as

$$\mathcal{B}_{(i,j)} = \frac{I_{(i,j)}(\mathrm{Exp}) \times \mathcal{F}_{(\mathrm{i,j})}}{I_{R(i,j)}} \sum_{\mathrm{subset}} \frac{I_{R(i,j)}}{I_{(i,j)}(\mathrm{Exp}) \times \mathcal{F}_{(i,j)}}. \tag{4}$$

In Table 2, we compare the experimentally obtained data with the estimated abundance. The (7,6) tube dominates the subset investigated although its measured RBM intensity only accounts for 20% of the overall intensity. The strong deviations are mainly attributed to $\mathcal{M}_{22}$, as it depends significantly (up to a factor of five) on nanotube chirality.

4 Discussion and conclusion Figure 6 compares relative intensities measured with the two spectroscopic methods (the scaling to maximum resonance for the Raman intensities is already included) and the relative abundance including the estimated parameters. After correction both methods agree on the (7,6) species dominating the subset. The (7,5) and (10,3) species each account for less than 16%. The abundance obtained from PL and PLE is hardly altered by the estimated parameters. In the case of the Raman studies, especially M_{22} highly affects the estimated abundance. The (7,6) tube shows the lowest measured relative Raman intensity (20%), but due to its relatively low electron–phonon coupling it accounts for 84% of the nanotubes within the subset.

In conclusion, we estimated the relative abundance of three HiPCO semiconducting CNT species by comparing PL and Raman spectroscopy signal intensities. The obtained intensities were scaled using Raman resonance profiles as well as theoretical calculations on the electron–phonon coupling for Raman and excitonic transition probabilities for PL, PLE and Raman. After corrections both methods agreed

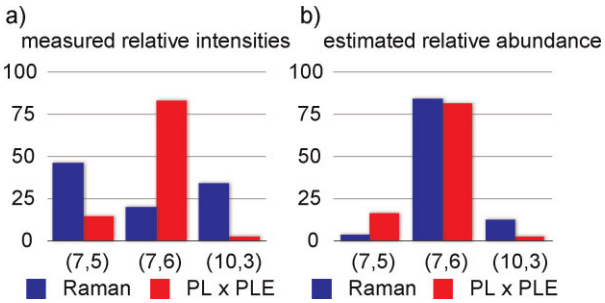

Figure 6 (online colour at: www.pss-b.com) (a) Relative signal intensities obtained by Raman (blue, scaling to full resonance included) and PL (red) measurements. (b) Estimated abundance including corrections.

on one species dominating the subset whereas the other two species each accounted for less than 16%. In particular, the Raman intensities strongly depended on electron–phonon coupling matrix elements $\mathcal{M}_{22}$. As the ratio between PL and PLE intensities varied for the different species, we proposed the product of PL and PLE intensities as a measure for quantitative analysis of CNT chiralities by PL.

Acknowledgements We thank J. Abrahamson and M. Strano for supply with CNTs and H. Telg for sending additional experimental data. This work was supported by ERC grant no. 210642.

References

[1] S. Iijiama, Nature **354**, 56 (1991).
[2] S. Reich, C. Thomsen, and J. Maultzsch, Carbon Nanotubes: Basic Concepts and Physical Properties (Wiley-VCH, Berlin, 2004).
[3] S. M. Bachilo, M. S. Strano, and C. Kitrell, Science **298**, 2361 (2002).
[4] Y. Miyauchi, S. Chiashi, Y. Murakami, Y. Hayashida, and S. Maruyama, Chem. Phys. Lett. **387**, 198 (2004).
[5] E. Malić, Many-particle theory of optical properties in low-dimensional nanostructures, Dissertation, Tu Berlin (2008). URL: http://opus.kobv.de/tuberlin/volltexte/2008/2058/
[6] S. Reich, C. Thomsen, and J. Robertson, Phys. Rev. Lett. **95**, 077402 (2005).
[7] Y. Oyama, R. Saito, and K. Sato, Carbon **44**, 873 (2006).
[8] J. Lefebvre, S. Maruyama, and P. Finnie, in: Carbon Nanotubes, Topics in Applied Physics, Vol. 111, edited by A. Jorio, M. Dresselhaus, and G. Dresselhaus (Springer, Heidelberg, 2007), Chap. 9
[9] J. Maultzsch, H. Telg, S. Reich, and C. Thomsen, Phys. Rev. B **72**, 205438 (2005).
[10] H. Telg, J. Maultzsch, S. Reich, F. Hennrich, and C. Thomsen, Phys. Rev. Lett. **93**, 177401 (2004).
[11] J. Jiang, R. Saito, Ge. G. Samsonidze, S. G. Chou, A. Jorio, G. Dresselhaus, and M. S. Dresselhaus, Phys. Rev. B **72**, 235408 (2005).